Materials Advances

ROYAL SOCIETY OF CHEMISTRY

PAPER

View Article Online
View Journal | View Issue

Cite this: *Mater. Adv.*, 2020, 1, 3339

Ultra high molecular weight polyethylene with incorporated crystal violet and gold nanoclusters is antimicrobial in low intensity light and in the dark

Ke Wu, [a] Gaowei Wu, [b] Alexander J. MacRobert,[c] Elaine Allan,[d] Asterios Gavriilidis [b] and Ivan P. Parkin *[a]

Antibiotics lose their effectiveness over time due to antimicrobial resistance. The increasing risk of hospital-acquired infections from contaminated surfaces and medical interventions requires the development of new antimicrobial materials. We report the first example of a modified ultra high molecular weight polyethylene that showed good antibacterial properties on light activation. Its efficacy was due to the production of reactive oxygen species under low-intensity white light sources (*ca.* 375 lux). Crystal violet and cysteine capped gold nanoclusters were successfully incorporated into the polymer using a readily available solvent as a dispersing agent followed by the process of compression moulding at 200 °C, 4.5 MPa for 1 min. This modified ultra-high molecular weight polyethylene demonstrates excellent robustness with regards to dye and metal leaching as well as photostability. Despite incorporating antimicrobial agents, the modified ultra-high molecular weight polyethylene retained its mechanical properties and showed >99% reduction in bacterial numbers against *Escherichia coli* and. To our knowledge, this paper reports the first use of compression moulding to create a light-activated antimicrobial surface which has distinct processing advantages over the widely used "swell-encapsulation-shrink" method and is potentially scalable.

Received 16th September 2020,
Accepted 4th November 2020

DOI: 10.1039/d0ma00710b

rsc.li/materials-advances

Introduction

In a hospital environment, pathogenic microbes can be transmitted from an infected patient *via* aerosol generation and subsequently adhere to surfaces. Patients, healthcare personnel and visitors are at risk of becoming pathogen carriers by touching contaminated inanimate surfaces such as countertops, doorknobs and handrails which can harbour Gram-positive and Gram-negative bacteria for more than six months.[1] Patients who have weakened immune systems, such as haematology and cancer patients, are particularly susceptible to hospital-acquired infections (HAIs) that result in increased suffering and increased length of hospital stay, which incurs significant costs.[2] This associated cost continues to escalate at an alarming rate. For the USA, more than $30 billion is spent each year on HAIs, and these are implicated in 99 000 deaths.[2–4] In the European Union, it is estimated that more than 4 million patients contract HAIs per annum resulting in approximately 11 000 deaths.[5] The high rate of HAIs is further compounded by the increasing problem of antimicrobial resistance.

The implementation of antimicrobial surfaces into hospitals is one strategy to potentially reduce transmission of bacterial pathogens between patients.[6] Emerging technologies used to fabricate coated surfaces with antimicrobial properties typically use organic compounds or inorganic metals,[7–10] such as thin films that release antibiotics,[11] copper incorporated polymers[8,12] and organic biocide entrapped coatings.[13] An alternative solution is the development of light-activated microbicidal surfaces.[7,14–16] A photosensitizer, when subjected to light in the visible region of the electromagnetic spectrum, generates cytotoxic reactive oxygen species (ROS) that can ultimately lead to bacterial cell death.[6,15,17] The process is historically known as either 'Type I' and 'Type II' mechanism involving the interaction of excited triplet chromophore with molecular oxygen, water and target cellular biomolecules.[18–20] The interaction subsequently produces a wide range of ROS including free radicals and singlet oxygen. In both types of mechanism, the ROS generated targets multiple sites in

[a] *Department of Chemistry, University College London, 20 Gordon Street, London, WC1E 0AJ, UK. E-mail: i.p.parkin@ucl.ac.uk*
[b] *Department of Chemical Engineering, University College London, Torrington Place, London, WC1E 7JE, UK*
[c] *Division of Surgery & Interventional Science, University College London, Charles Bell House, 43-45 Foley St., London, W1W 7TS, UK*
[d] *Department of Microbial Diseases, UCL Eastman Dental Institute, Royal Free Campus, University College London, Rowland Hill Street, London, NW3 2PF, UK*

the bacterial cell which reduces the likelihood of antibacterial resistance.[19,20]

Metal nanoparticles such as gold and zinc oxide are known to enhance the effectiveness of photosensitisers.[7,14,16,21] Noimark *et al.* demonstrated that 2 nm gold nanoparticles (AuNPs) in combination with a commercially available photosensitizer, crystal violet (CV), in a silicon polymer fabricated *via* a ''swell-encapsulation shrink'' method had significant bactericidal activity.[15] For both *Staphylococcus epidermidis* and *Escherichia coli* (*E. coli*), *ca.* 2 log reduction in bacterial number was achieved after 3 h and 6 h respectively, following exposure to 4000 lux white light.[15] Furthermore, Macdonald *et al.* and Perni *et al.* demonstrated that the addition of AuNPs enhanced the antimicrobial properties of the light-activated surfaces in a size-dependent manner, with the smallest gold nanoparticles showing the greatest synergistic effect with the dye.[16,22] Recent research also explored the broad-spectrum antimicrobial activity of solutions of ultra-small gold nanoclusters.[23] The study showed that a 0.1 μM gold nanocluster (AuNCs) solution exhibited roughly 1.3 log reduction in bacterial number against *S. aureus* and a 1.4 log reduction for *E. coli* after 2 h treatment.[23] Recent studies within our group showed that the photoactivated gold nanocluster embedded polyurethane upon 6 h white light irradiation exhibited more than 3.3 log for *S. aureus* while *E. coli* required 4-fold longer exposure time with roughly 2.8 log reduction in bacterial numbers.[24]

Ultra high molecular weight polyethylene (UHMWPE) shows low abrasion, robust mechanical properties and is largely chemically inert. These characteristics enable it to be applied in diverse areas including conveying,[25] maritime industry, textiles[26] and automotive. Moreover, its outstanding biocompatibility makes it a suitable candidate for orthopaedic materials.[27,28] One approach to make wear resistance hard antimicrobial surfaces is to modify the UHMWPE. The existing work on antimicrobial UHMWP includes depositing a copper coating on UHMWPE *via* aerosol assisted chemical vapor deposition (AACVD).[29] Della Side *et al.* developed an antimicrobial titanium oxide coated UHMWPE.[30] However, the main drawback is the requirement of a laser source to activate the coating during the implantation process. Moreover, high dose laser pulses might potentially bring in an adverse effect on the mechanical properties of the modified UHMWPE.[31] Other research groups have investigated the antimicrobial mechanism of ZnO reinforced UHMWPE nanocomposite.[32] ZnO nanoparticles exhibit dark kill through releasing H_2O_2 and Zn^{2+}.[32] The material demonstrated *ca.* 80% kill of *E. coli* and 74% of *Staphylococcus aureus* (*S. aureus*) for 4 h incubation time with a high content of the nanoparticles (20% w/w).[32]

While the material is potentially targeted towards clinical applications, it is critical that the antimicrobial moiety within the polymer maintain non-toxicity towards mammalian cells. Crystal violet, also known as gentian violet, is non-toxic to mammalian cells.[7] According to Maley *et al.*, the use of crystal violet showed no toxicity to humans.[33] Historically, crystal violet has been used to treat dermatology conditions including scratch wound healing, oral candidiasis and fungal skin infection due to its potent antimicrobial and antifungal properties.[7,34,35] Metal nanoparticles demonstrate antimicrobial properties attribute to the generation of metal ions; a good example is silver nanoparticles. However, the cytotoxicity towards bacterial cells is also compromising the mammalian cells, which result in poor biocompatibility. The highly stable Au NPs, however, has proved to be biocompatible in the mammalian system, both *in vitro* and *in vivo*.[36] The biocompatibility extended towards smaller size AuNCs.[23] Previous research has demonstrated AuNCs did not cause any damage to human cells.[23,37] Together, these provide the possibility to ensure clinical translation in the future.

Herein, we developed an environmentally and economically sustainable method to manufacture photoactivated antimicrobial hard surfaces by incorporating crystal violet and cysteine capped Au_{25} nanoclusters ($Au_{25}Cys_{18}NCs$) into powdered UHMWPE through a simple compression moulding process. The high molecular weight of the polymer results in high melt viscosity, therefore a pressurized powder sintering preparation method was adapted.[38] Antimicrobial agents that can endure high-temperature manufacturing process are desirable. Crystal violet is a promising compatible candidate as it melts around 205 °C. As described below, the $Au_{25}Cys_{18}NCs$ survived the compression moulding procedure despite the relatively high processing temperature. The CV and $Au_{25}Cys_{18}NCs$ incorporated UHMWPE only had trace amounts ($\geq$0.1% w/w) of the antimicrobial agents yet maintained good mechanical properties and presented outstanding antimicrobial activity at light levels commonly seen in hospital wards. This is a particularly promising approach due to its multi-target mode of action and reduced risk of resistance development.[17,39]

Materials and methods

Gold nanocluster synthesis

The $Au_{25}Cys_{18}NCs$ were synthesized using a method adapted from the literature described by Huang *et al.*[40] The Au precursor (10 mM) was prepared by mixing the $HAuCl_4$ with cysteine in a 1 : 1.5 molar ratio in deionized water at a pH adjusted to 12 by NaOH. All chemicals were of analytical grade and purchased at Sigma Aldrich. A tube-in-tube reactor was set up with an inner Teflon AF-2400 tube (inner diameter (ID), 0.8 mm; outer diameter (OD), 1.0 mm; Biogeneral) and an outer PTFE tube (ID, 2.4 mm; OD, 3.2 mm; VICI Jour). The total length of the reactor was 2 m, and the volume of the inner tube was 1 mL. The reactor was kept in an oil bath at 80 °C. The Au precursor solution was input into the inner tube at a speed of 0.33 mL min^{-1} by using a milliGAT pump, and the outlet of the inner tube was connected to a back-pressure regulator (BPR, Zaiput) maintained at 6 bars. Gaseous CO was connected to the annulus between the inner and outer tube *via* a T-junction, and the CO pressure was maintained at 5 bar throughout the process. The $Au_{25}Cys_{18}NCs$ solution was collected from the outlet of the reactor and directly used without further purification.

Preparation of UHMWPE surfaces

UHMWPE surfaces were prepared *via* compression moulding. The virgin UHMWPE powder (M_w: average 3 000 000–6 000 000) was compressed in a mould with dimension 56.5 × 50.0 mm by using vulcanizing press Type VP 6G (SEBA Developments) at 200 °C and 4.5 MPa for 1 min. The resulting consolidated UHMWPE composite was cooled down to room temperature to yield a ~2 mm thick white UHMWPE thin sheet.

Preparation of CVAuNC UHMWPE

The desired amount of CV and Au NCs were mixed in a 3 mL of a mixture of water/ethanol mixture (volume ratio, 2 : 1), and blended with 5 g of UHMWPE powder. The obtained slurry was dried overnight, at room temperature in the dark. The dried CVAuNC UHMWPE powder was consolidated *via* compression moulding described above.

In order to optimize the amount of $Au_{25}Cys_{18}$NCs used, 0.005% w/w, 0.01% w/w, 0.05% w/w and 0.1% w/w of the $Au_{25}Cys_{18}$NCs was added to 0.1% w/w CV in UHMWPE powder respectively using water/methanol mixture as a dispersing solvent. *Vice versa*, for optimizing the amount of CV, 0.05% w/w, 0.1% w/w and 0.5% w/w of CV was mixed with 0.05% w/w the $Au_{25}Cys_{18}$NCs solution respectively with the rest of the procedures as above.

CVAuNC UHMWPE characterization

Scanning electronic microscopy (SEM) (JEOL JSM-6301F) was used to investigate the surface structure of control and modified UHMWPE before and after the consolidation at an accelerating voltage of 10 kV. Transmission electron microscopy (TEM) (JEOL 2010) was used to visualize the samples' crystalline morphology. The UHMWPE coupons were cut by ultramicrotome (Reichert Jung Ultra cut E 701701) with thickness less than 100 nm and loaded onto holey carbon-coated copper grids (Agar Scientific Ltd) prior to staining by UranyLess EM Stain for 45 s. Image collection and processing were performed by Gatan Digitalmicrograph software. X-Ray diffraction (XRD) (Bruker D8 Discovery X-ray diffractometer) was used to obtain the crystal phase of the polymers in a diffraction angle range between 10–66 °C using a monochromatic CuKα (λ = 1.5406 Å) radiation at 40 kV voltage and 40 mA current power supply. A differential scanning calorimeter (DSC) (Netzsch STA 449 C Jupiter Thermo-microbalance) was used to determine thermal transitions of the polymers. Data analysis was carried out by using Netzsch Preteus. The theoretical heats of fusion of 100% crystalline UHMWPE, ΔH_f = 289.3 J g^{-1} have been used throughout the analysis. For all characterizations that had been carried out ''CVAuNC UHMWPE'' refers to a sample containing 0.05% w/w of AuNC and 0.1% w/w CV.

Characterization of photosensitizer uptake

The CV distribution within the UHMWPE matrix was examined using optical microscopy. Samples were deposited vertically in paraffin blocks. Each paraffin block with polymer inlay was sliced into 6 μm sections using a microtome (Leica RM2235). These thinly sliced sections were subsequently imaged using a light microscope (GXML 3230, GT Vision Ltd).

Antimicrobial assay

The effectiveness of CVAuNC UHMWPE composites in eradicating *S. aureus* 8325-4[41] and *E. coli* ATCC 25922 under low-intensity white light was investigated. In order to optimize the $Au_{25}Cys_{18}$NCs concentration in the CVAuNC composite, each bacterium was exposed to control UHMWPE, CV UHMWPE and CVAuNC UHMWPE with various concentrations of the $Au_{25}Cys_{18}$NCs. Both CV UHMWPE and CVAuNC UHMWPE contain the same amount of CV (0.1% w/w). For optimizing the concentration of CV in CVAuNC UHMWPE, each of the bacterial cultures was exposed to control UHMWPE and CVAuNC UHMWPE containing various amounts of CV but with constant $Au_{25}Cys_{18}$NC concentration (0.05% w/w).

For each species, one bacterial colony was inoculated into BHI (Brain Heart Infusion) broth (Fisher Scientific) (10 mL) and cultured aerobically at 37 °C 200 rpm (4500 g) for 17 h. The bacterial pellet was washed twice in PBS (10 mL) after which it was resuspended in PBS (10 mL). The inoculum was obtained (~10^6 CFU mL^{-1}) by diluting the suspension 1000-fold in PBS. For each set of experiments, 25 μL of the inoculum was exposed to 1 × 1 cm sample in a humidity chamber. Duplicates of each sample type were used. All samples were then irradiated under a white light source with an average intensity of 375 lux for either 6 (*S. aureus*) or 24 h (*E. coli*). A further set of samples (in duplicate) was maintained in the dark for the same duration as the illuminated samples. Post irradiation, each sample was added to PBS (450 μL) and vortexed. The bacterial suspensions were ten-fold serially diluted and plated on to agar for viable counts. The plates were incubated aerobically at 37 °C for 24 hours (*E. coli*) and 48 hours (*S. aureus*). Each experiment was repeated three times. Statistical significance was determined using the Mann–Whitney *U* test.

Functional testing

All materials investigated were cut into Type IV dumbbell-shaped specimen in accordance with ASTM D638-12 by laser cutter (Trotec Speedy 100R). Tensile tests for each sample type (n = 5) were performed by using a tensile testing machine (Instron 5565) at a stretching speed of 100 mm min^{-1}.

The leaching effect of CVAuNC UHMWPE in phosphate buffer saline (PBS) (OXOID) was investigated at room temperature. The CV leaching was tested by placing each of the 3 CVAuNC UHMWPE coupons (1 × 1 cm) in separate bottles containing 2.5 mL PBS for up to 20 days. On days 1, 5, 10, 15 and 20, 0.5 mL of PBS in each bottle was removed for measurement by UV-Vis absorbance at 590 nm (Pharmacia Biotech Ultrospec 2000) and an equivalent amount of fresh PBS was added back to each bottle. A calibration curve was set up by determining the absorbance at 590 nm of known concentrations of CV solution and their corresponding absorbance at 590 nm. The gold leaching from CVAuNC UHMWPE into PBS was determined with Microwave-Plasma Atomic Emission Spectroscopy (MP-AES 4210, Agilent). The procedures were the

same as above, except 25 mL of PBS was used and 5 mL of eluted PBS was removed for analysis with the same amount of fresh PBS refilled.

The photostability of CVAuNC UHMWPE under white light irradiation was examined spectroscopically. The control and modified UHMWPE samples were stored in a box with a continuous and constant light source (General Electric 28 W Watt Miser™T5 2D compact fluorescent lamp) emitting an average white light intensity of 3000 ± 125 lux for an extended period, and samples were characterized by using the same UV-vis spectrometer periodically.

The water contact angle of the CVAuNC UHMWPE surface was determined by averaging the values of 5 different measurements at various places on the sample. Each of the equilibrium water contact angles was measured by dispensing a water droplet (5 μL) under gravity using a FTA 100 Optical Contact angle meter. Side on image was taken and subsequently analysed using FTA32 software.

Results and discussion

The intrinsically high density of UHMWPE makes it largely unsuitable for incorporating any antimicrobial agents through the swell-encapsulation-shrink method.[42,43] Thus a new method was developed using powdered UHMWPE and encapsulating CV and the $Au_{25}Cys_{18}$NCs to the powder before consolidation by compression moulding. The dye and metal nanocluster were added to a minimal amount of water/methanol mixture, which was then blended with virgin UHMWPE powder. A purple coloured UHMWPE powder was obtained after overnight drying. The powder was then consolidated into a rectangular stainless-steel window (inner size: 56.5 × 50.0 mm, outer size: 81.3 × 74.5 mm) by compression moulding at 200 °C.

The molecular structure of UHMWPE can be visualized as an extended long twisted string.[44] During the compression moulding process but below the melting temperature, the molecular chain is likely to rotate about the long carbon–carbon bonds forming chain folds.[44] These chain folds allow the molecule to form layers of highly oriented crystalline lamellae which act as inlays within the disordered amorphous regions.[44] This crystalline morphology is microscopic usually the inlays have a thickness of order of 10 to 50 nm which can be visualized by TEM. Thus, the compressed moulded UHMWPE control and optimized CVAuNC UHMWPE were cut by ultramicrotome with thickness controlled to below 100 nm. Fig. 1a and b show the TEM micrographs of UHMWPE control and CVAuNC UHMWPE. There is no observable distinction between two samples which indicates the incorporation of phenothiazine dye CV and $Au_{25}Cys_{18}$NC does not affect the morphology of the polymer. In both TEM micrographs, the amorphous structure was represented by the grey region, whereas the lamellae (ordered region) appeared as dark floccule. The surface morphology for both control and CV AuNC incorporated UHMWPE were investigated using SEM. Fig. 1c and d show the low-resolution SEM micrographs prior and after the incorporation of CV and AuNC. The embedded CV and AuNC have not changed the polymerization with each UHMWPE particle, size approximately 150 microns, closely packed.

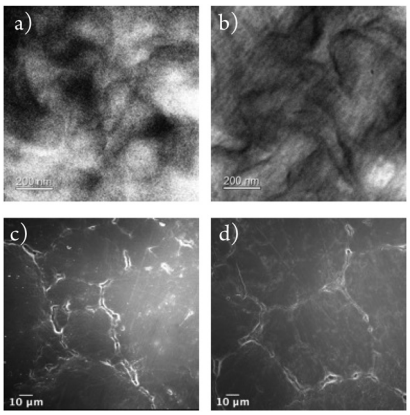

Fig. 1 TEM images showing (a) UHMWPE control material and (b) CVAuNC UHMWPE; (c) and (d) show SEM images of UHMWPE control and CVAuNC UHMWPE respectively each with 600× magnification.

The mechanical properties of UHMWPE are related to its crystalline structure.[45] Hence, any phase modification may alter the mechanical behaviour of the material.[45] The process of crosslinking the amorphous region might result in changing the crystallinity and therefore affect the mechanical behaviour.[45] Phase characterization of compression moulded UHMWPE control and CVAuNC UHMWPE were examined using XRD. Semi-crystalline UHMWPE has a diffraction pattern consists of both sharp diffraction maxima and dispersed scattering as a result of amorphous phase across a wide range of diffraction angle.[46] In Fig. 2, both X-ray patterns have signature peaks that arise at 2θ values of 21°, 23° and 36° which are attributed to the (1 1 0), (2 0 0) and (0 2 0) crystal planes respectively. Fig. 2 inset shows an example of the overlap

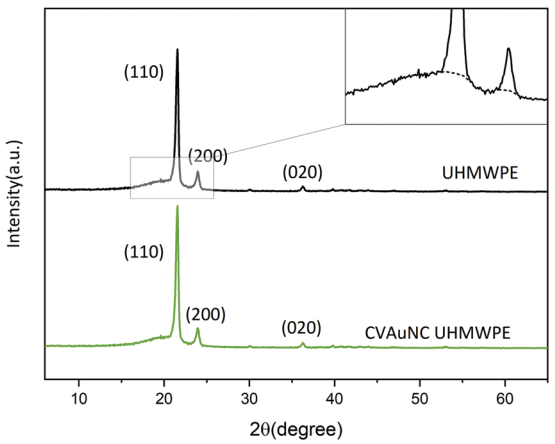

Fig. 2 X-Ray diffraction plots of ultra-high molecular weight polyethylene control and crystal violet gold nanocluster embedded ultra-high molecular weight polyethylene sample measured across 2θ range from 6 to 66°. A small section of the diffraction pattern of the UHMWPE was shown by a zoomed inset shown on the top right.

between the two intense diffraction maxima due to the ordered crystalline phase and the diffused scattering (below the dashed line) due to the amorphous phase. The percentage crystallinity in the polymer can be estimated as the ratio of total integral intensities of the crystalline peaks to the total integral intensities of amorphous and crystalline peaks and linear background (see eqn (1)). The calculated UHMWPE control had 70.47% crystallinity, whereas the CVAuNC samples had 70.07%. The percentage crystallinity after the incorporation of effective antimicrobial agents had a 0.05% difference which is negligible. Hence, we can postulate that the modified UHMWPE largely retains its crystalline properties regardless of the incorporation of the antimicrobial agents.

$$\%\ \text{crystallinity} = \left(\frac{I_c}{I_c + I_a}\right) \times 100\%. \quad (1)$$

I_c: total integral intensities of crystalline peaks; I_a: total integral intensities of amorphous.

DSC was employed to estimate the material's melting temperature and crystallinity. Samples were heated up to 250 °C at a rate of 25 °C min^{-1}. Fig. 3 shows the thermogram of both UHMWPE control and CVAuNC UHMWPE samples. Each peak showed between 100–175 °C was defined by an onset, offset and peak temperature. The peak temperature (T_p) was designated by the extrapolated intersections of the tangents of both onset (T_{on}) and offset (T_{off}) temperatures in the endothermic peak on the thermogram. An example is shown in Fig. 3, where the UHMWPE control peak temperature is at the intersection of the two dashed lines. When melting pure materials, the T_{on} usually equates to the melting temperature (T_m). However, this is not the case for polymers. Since UHMWPE is a semi-crystalline polymer, it can show both first-order and second-order transition states which correspond to crystalline and amorphous regions respectively during the phase change.[47] The peak melting point is the characteristic temperature of the first-order transition at which bulk crystallites melt.[44,48] Therefore, the UHMWPE has a true melting temperature at T_p where the ordered crystallites turn into a disordered phase.[48] The control and CVAuNC UHMWPE have T_p 137.7 °C and 138.2 °C (Fig. 3) respectively which are quite close to values reported in the literature (137.28 °C).[44] As this parameter is highly dependent on the sample crystallinity,[49] further investigation was carried out to estimate the percentage crystallinity. The crystallinity of the sample was obtained by integrating the enthalpy peak from 50 to 160 °C which was then subsequently normalized to the heat of fusion of 100% crystalline polyethylene (289.3 J g^{-1}) according to the standard ASTMF2625-10 (see eqn (2)). The calculated percentage crystallinity of UHMWPE control was 68.99%, whereas the CVAuNC UHMWPE was 72.55%. It was observed that with the addition of CV and AuNC, the crystallinity showed around a 5% change. Overall, the estimated crystallinity obtained from DSC analysis was consistent with the above XRD analysis.

$$\%\ \text{crystallinity} = \frac{\Delta H_s}{\Delta H_f} \times 100\% \quad (2)$$

ΔH_f: the theoretical heat of fusion of 100% crystalline material in J g^{-1}; ΔH_s: the heat of fusion of tested material in J g^{-1}.

To investigate the dye distribution within the polymeric matrix, the prepared UHMWPE surfaces with and without the incorporation of crystal violet were analysed by light microscopy. Fig. 4a and b display the morphology of thinly sliced control and CVAuNC UHMWPE. Both images indicate individual UHMWPE particles closely packed together, and the size varies from 100–150 μm. Fig. 4b indicates that instead of diffusing throughout each PE particle, the dye agglomerates at the particle edge.

Antimicrobial assay

In order to determine the most effective concentration of each antimicrobial agent in UHMWPE, experiments were conducted with varying relative concentrations of dye and gold cluster. For optimizing the $Au_{25}Cys_{18}NC$ amount incorporated in the polymer, 0% w/w, 0.005% w/w, 0.01% w/w, 0.05% w/w and 0.1% w/w of $Au_{25}Cys_{18}NCs$ were blended with UHMWPE powder using 0.1% w/w of CV dissolved in water–methanol mixture as a dispersing solution. The solvent was evaporated overnight prior to consolidation. Similarly, for determining CV concentration, a known amount of $Au_{25}Cys_{18}NCs$ was used from the above study

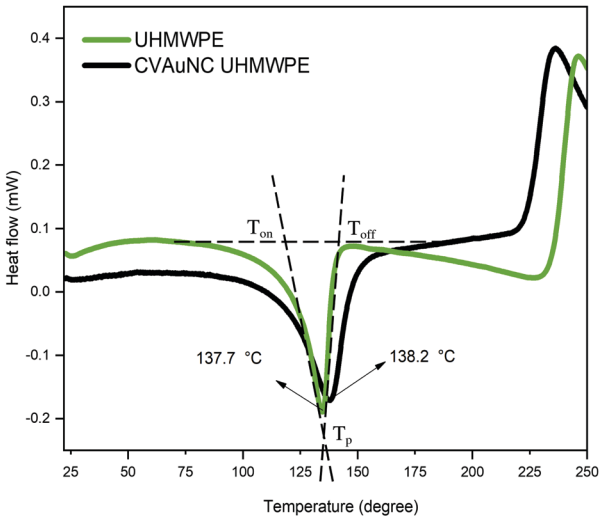

Fig. 3 Differential scanning calorimetry profiles of ultra-high molecular weight polyethylene and crystal violet gold nanocluster embedded ultra-high molecular weight polyethylene. Peak temperatures are indicated by the arrow shown on the figure.

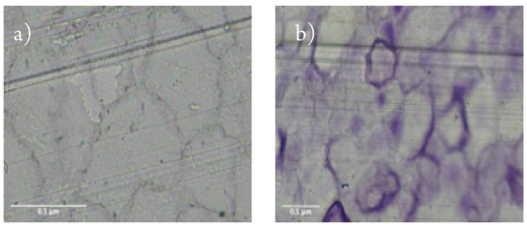

Fig. 4 Images showing cross sections of compression moulded (a) ultra-high molecular weight polyethylene control and (b) crystal violet gold nanocluster embedded ultra-high molecular weight polyethylene.

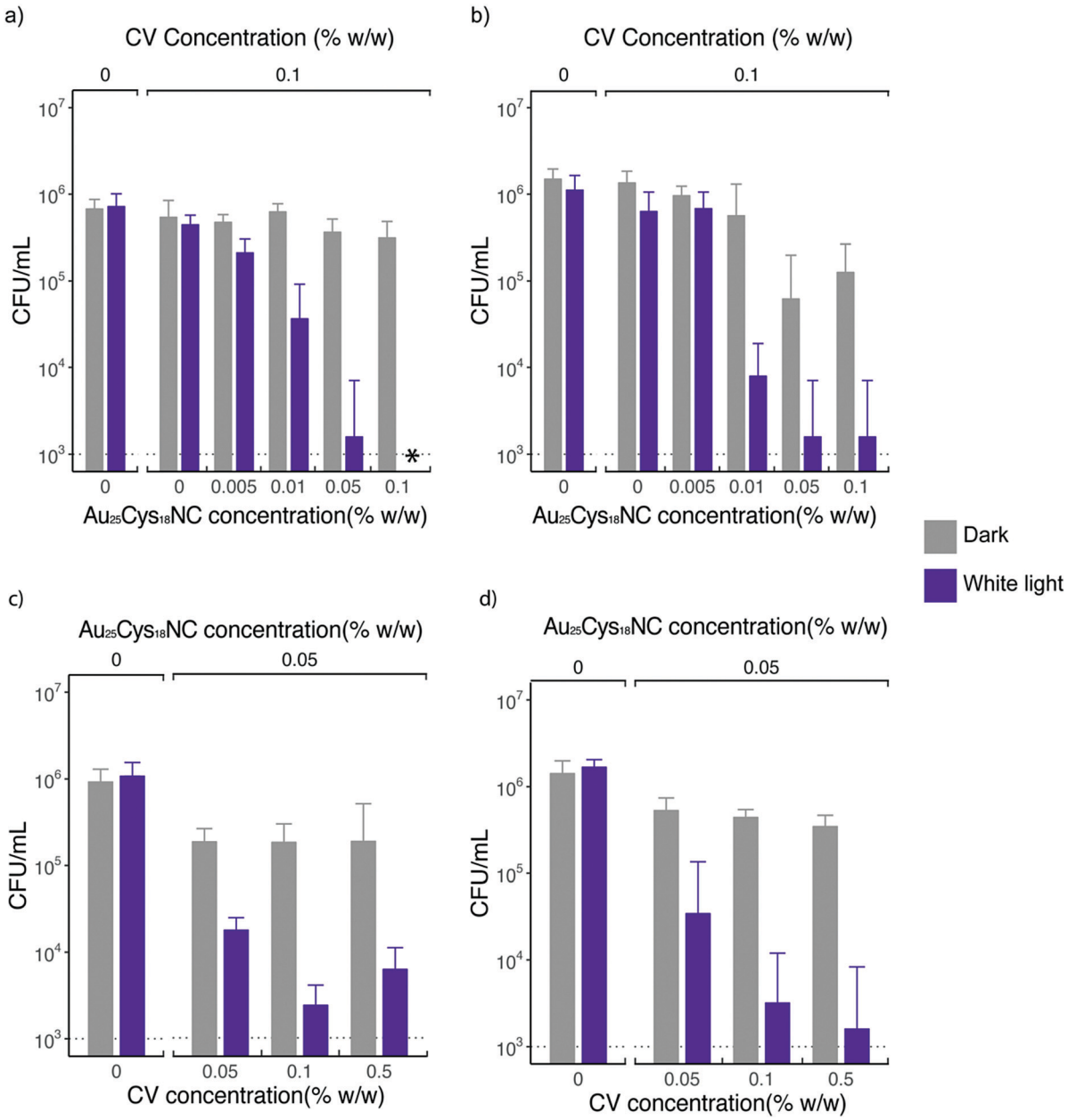

Fig. 5 Antimicrobial activity of the CVAuNC UHMWPE against (a) and (c) *Staphylococcus aureus* upon white light irradiation and in dark for 6 h; (b) and (d) *Escherichia coli* upon white light irradiation and in dark for 24 h. The white light had an average intensity of 375 ± 25 lux. A control UHMWPE (indicated by 0% w/w CV concentration and AuNC concentration) was used throughout the antimicrobial assay. In (a) and (b) CVAuNC UHMWPE samples with increasing concentration of AuNC were used, all CV containing samples has CV concentration constant at 0.1% w/w. In (c) and (d) CVAuNC UHMWPE samples had CV concentration increasing while the amount of $Au_{25}Csy_{18}NC$ constant at 0.05% w/w. The asterisk indicates the bacterial counts are below detection limit (1000 CFU mL^{-1}). The inoculum used in each assay for both strains was to the tune of $\sim 10^6$ CFU mL^{-1}.

while making CVAuNC UHMWPE composite with various CV concentrations. Samples, including a UHMWPE control, were exposed to both Gram-positive and Gram-negative bacteria, *S. aureus* and *E. coli*, respectively. A white light source with an intensity of 375 lux ± 25 was used which is, by far, one of the lowest degrees of illuminance that has been used to activate photoactive antimicrobial surfaces (typically 1000–10 000 lux or laser light is used).

Fig. 5a shows the bactericidal effect of CV UHMWPE and CVAuNC UHMWPE with 0.1% w/w CV and various concentrations of $Au_{25}Cys_{18}NCs$ upon irradiation with constant white light for 6 h against *S. aureus*. CV UHMWPE demonstrated a small yet statistically significant reduction (0.21 log) in bacterial numbers compare to UHMWPE control ($p < 0.01$). The presence of the $Au_{25}Cys_{18}NCs$ resulted in an enhancement in the photoactivated antimicrobial activity of the prepared surfaces. A positive correlation between the photoactivated bactericidal activity and the gold nanocluster concentration was observed at a fixed CV concentration. For the sample that contained 0.05% w/w of $Au_{25}Cys_{18}NCs$, a 2.66 log reduction in bacterial

numbers ($p < 0.001$) was apparent whereas with 0.1% w/w of $Au_{25}Cys_{18}$NCs the number of surviving bacteria was below the detection limit (1000 CFU mL^{-1}). It was also noticed that samples with an $Au_{25}Cys_{18}$NCs content above 0.05% w/w (with 0.1% w/w CV) exhibited low level but statistically significant bactericidal activity (>0.27 log reduction) ($p < 0.01$) in the dark. According to Zheng *et al.* AuNCs has intrinsic antimicrobial properties.[23] It is believed that the AuNC itself can induce a metabolic imbalance to the bacterial cell by increasing the expression levels of genes that associate with the release of ROS as byproducts.[23] In contrast, it can decrease the expression of the *Gaphd* gene which involved in the elimination of ROS.[23] Moreover, the nanoclusters can inflict damage directly on the bacterial cell membrane.[23]

When tested against *E. coli*, the prepared surfaces exhibited enhanced antimicrobial activity with $Au_{25}Cys_{18}$NC content increasing (shown in Fig. 5b) after 24 h exposure time. However, increasing the concentration above 0.5% w/w (~2.85 log kill) did not achieve any further increase in bactericidal activity. The CV UHMWPE sample did not show a significant reduction in bacterial number ($p > 0.05$) upon incubation under the dark condition for 24 h. However, with the addition of $Au_{25}Cys_{18}$NC, the CVAuNC UHMWPE samples demonstrated significant antimicrobial efficacy with higher $Au_{25}Cys_{18}$NC concentrations (>0.05% w/w) giving greater bactericidal activity. For the two CVAuNC UHMWPE samples with AuNC concentration above 0.05% w/w, a more than 1 log reduction in bacterial numbers ($p < 0.01$) was observed. Since almost 3 log reduction was achieved with 0.05% w/w in the light and activity was even apparent in the dark, this concentration was selected in the interests of cost.

To determine the most effective CV concentration required, 0.05% w/w, 0.1% w/w and 0.5% w/w of CV were incorporated into the UHMWPE with the addition of 0.05% w/w AuNC in each of the CV UHMWPE composites, and the samples were tested using the same strains of *S. aureus* and *E. coli*. Fig. 5c and d shows the antimicrobial activities of CVAuNC UHMWPE samples against *S. aureus* and *E. coli*, respectively. In general, increasing bactericidal activity was observed with increasing CV concentration upon illumination of white light. The three CVAuNC UHMWPE samples demonstrated 0.42, 0.51 and 0.61 log reduction in bacterial numbers ($p < 0.05$) respectively, against *S. aureus* in the dark (Fig. 5c). A further enhancement was observed in antimicrobial activity when white light was used to strike the photoactivated antimicrobial surfaces. The CVAuNC UHMWPE samples with CV concentration 0.1% w/w showed *ca.* 2.66 log reduction in bacterial numbers upon 6 h white light illumination, whereas there was no significant difference between the samples containing 0.1 and 0.5% w/w of CV, each achieving 2.2–2.7 log reduction in bacterial numbers. In Fig. 5d, a similar trend was apparent with all CVAuNC UHMWPE samples showing more than 0.42 log kill in the dark. Overall, the results showed, unsurprisingly, that higher CV concentrations resulted in increased bactericidal activity. Since no significant increase in bacterial kill increase was observed at 0.5% w/w compared to 0.1% CV, the lower concentration was chosen as the optimum concentration used in the CVAuNC UHMWPE composite.

Although the AuNCs is intrinsically antimicrobial, it is speculated that the contribution towards the overall antimicrobial activity of the CVAuNC UHMWPE under light condition is marginal. Since the AuNCs was embedded into the polymeric matrix, which limited the direct interaction with bacteria. It is also suggested that a synergy of antimicrobial efficacy was introduced with the combination of AuNC and photosensitiser dye. Recent research has been carried out within our research group that has revealed that the participation of AuNCs facilitates the generation of H_2O_2 and subsequent antimicrobial activity.[24] Previous light activated antimicrobial studies largely required high-intensity white light or high power laser sources to activate the dye and metal nanoparticle incorporated polymers.[7,14,16,21,50] Swell-encapsulated 2 nm AuNPs and CV polyurethane demonstrated a 2.2 log reduction in bacterial number when tested against the same strain of *E. coli* which was close to the activity displayed by the CVAuNC UHMWPE sample in this study.[16] However, a more intense white light source (>6000 lux) was required to activate the swell-encapsulated CVAuNP polyurethane sample which was 16-fold higher than the light source used in this study. The bactericidal activity displayed by compression moulded CVAuNC UHMWPE activated at low levels of white light suggests that $Au_{25}Cys_{18}$NCs is more effective than AuNPs in activating the photosensitizer encapsulated polymers.

Functional testing

A direct measure of the mechanical properties of optimized CVAuNC UHMWPE sample was carried out and the results are shown in Table 1. The tensile testing illustrates the incorporation of CV and AuNCs cause little change (~3 MPa decrement) in yield strength. The tensile strength, Young's modulus and elongation at break (ductility) and were observed to drop by 12.7%, 17.2% and 3.5% respectively.

The photostability of the crystal violet incorporated in modified UHMWPE samples upon irradiation was examined using UV-Vis spectroscopy. A white light source with intensity 3000 ± 130 lux was applied continuously for 1–20 days. The UV-Vis absorbance spectra (400–800 nm) of the illuminated samples were measured on day 1 and day 20. In Fig. 6, the sample

Table 1 Physical properties and mechanical study data for ultra-high molecular weight polyethylene control and crystal violet gold nanocluster embedded ultra-high molecular weight polyethylene samples

	Yield strength/MPa	Tensile strength/MPa	Young's modulus/MPa	Elongation at break/%
UHMWPE	20.65 ± 1.45	31.97 ± 3.69	366.98 ± 5.20	341.84 ± 26.50
CVAuNC UHMWPE	17.13 ± 0.67	28.35 ± 4.93	313.12 ± 6.22	330.02 ± 16.97

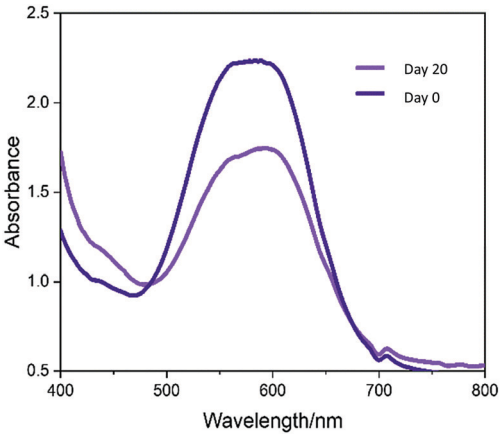

Fig. 6 UV-Vis spectra measured (400–750 nm) of crystal violet and gold nanocluster compressed moulded UHMWPE. The sample was stored in a light box with constant white light striking on the sample surfaces. The UV-vis absorbance was measured on day 1 and day 20 to investigate the photostability of the material after light exposure for an extended period.

shows good photostability with photodegradation of just 28% over the 20 days. When the material is exposed in an ambient environment with similar light intensity used in hospital for simple examination of the patients (*ca.* 300 lux),[51] it is postulated that the CV dye will retain its colour for at least three years. This is because the light source used during the photostability test has intensity roughly 10-fold higher than that of the ambient environment. From the above photostability test result, we speculate that it will take roughly 200 days for the CV to degrade by 28%.

The leaching effect of crystal violet from CVAuNC UHMWPE was spectroscopically investigated and plotted as a function of time. Samples were fully immersed in PBS in the dark for a period of up to 20 days. The optical density of the eluted aqueous solution was measured at 590 nm and subsequently converted into concentration (ppb) by using a calibration curve. Fig. 7 indicates that the sample upon immersion showed that a minimal amount of crystal violet leached out over the first 5 days. As time went on, the released crystal violet plateaued over time. At the end of the investigation, the leaching of the crystal violet from CVAuNC UHMWPE into the surrounding PBS was 0.93 ppb.

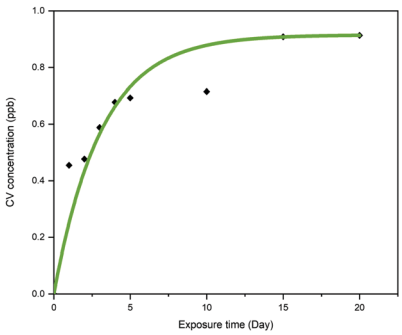

Fig. 7 The leaching of crystal violet (ppb) from a crystal violet gold nanocluster embedded ultra-high molecular weight polyethylene into phosphate buffer saline solution at room temperature was measured as function of time (day).

For the leaching of Au from the treated UHMWPE into PBS, no Au was detected in the solutions throughout the whole period (same Au concentration observed as the blank sample (<0.1 ppm)), which indicates no Au leaching from the surface. Overall, no colour change and no leaching of metal nanocluster was observed. This indicated that the antimicrobial agents were stably encapsulated into the UHMWPE matrix *via* compression moulding. The minimal level of leaching is likely due to surface adhered crystal violet and not that incorporated into the polymer.

Sharma *et al.* investigated the antimicrobial activity of ZnO nanoparticle encapsulated UHMWPE composite with various concentration of ZnO nanoparticle.[32] Samples demonstrated $\sim$75 and $\sim$80% kill (equivalent to 0.6 log and 0.7 log reduction in bacterial number) when tested against *S. aureus* and *E. coli*, respectively, with a ZnO concentration of 20% w/w.[32] However, the tensile strength and elongation at break had exceedingly contrasting values between untreated and treated UHMWPE with a decline of 81.3 and 180.1%. In comparison, the superior photoactivated crystal violet and gold nanocluster encapsulated UHWMPE demonstrated more than $>$99% kill when tested against the same strains as those used here with only a trace amount of antimicrobial agents. Besides, imperceptible change was observed in mechanical properties before and after the modification.

The water contact angle measurements of the unmodified and modified UHMWPE were measured to investigate the wettability of the material. For control and CVAuNC UHMWPE, the contact angles had values of 99° and 102°, respectively. Untreated UHMWPE powder is naturally hydrophobic, and this remains unchanged after consolidation. Moreover, it was found that there was negligible difference between the wetting properties of the UHMWPE control compared to CVAuNC UHMWPE.

Conclusion

In this paper, we introduced a practical application of AuNCs in preparing light-activated antimicrobial hard surfaces. Crystal violet and gold nanocluster have been successfully incorporated into UHMWPE through compression moulding. This is the first time that gold nanoclusters in combination with compression moulding has been used to create light-activated antimicrobial surfaces. The technique is versatile and could be made to create monoliths of virtually any desired shape. The materials demonstrated excellent antimicrobial property against both the Gram-positive bacterium, *S. aureus* and the Gram-negative, *E. coli*. The concentrations of CV and $Au_{25}Cys_{18}NC$ incorporated in UHMWPE were varied, in order to find the lowest concentrations for acceptable antimicrobial performance. They were found to be 0.1% w/w and 0.05% w/w, respectively. The presence of $Au_{25}Cys_{18}NC$ not only resulted in a significant enhancement of the photobactericidal effect of the dye but also enabled activation of the material with a low-intensity white light source. Upon irradiation (*ca.* 375 lux), the material exhibited *ca.* 2.66 log reduction in bacterial numbers for *S. aureus* and *ca.* 2.85 log for *E. coli* in 24 h.

Spectroscopic analysis revealed that the incorporated photo-activated dye had a 28% degradation in the 20 days at high-intensity light. This suggests the material, in theory, has more than three years of life span in a hospital setting. Moreover, the tensile testing also confirmed that the modified UHMWPE still retaining its mechanical behaviour after the incorporation of antimicrobial agents. This novel antimicrobial material provides excellent shape flexibility that can be used for various applications in healthcare environments.

Author contributions

The manuscript was written by K. Wu. G. Wu synthesized the gold nanocluster. E. Allan, A. MacRobert, A. Gavriilidis and I. P. Parkin supervised experiments. All authors have given approval to the final version of the manuscript.

Funding

This work was supported by EPSRC CDT (EP/L015862/1). G. Wu thanks the EPSRC for financial support (EP/M015157/1) through the Manufacturing Advanced Functional Materials (MAFuMa) scheme.

Conflicts of interest

The authors declare no competing financial interest.

Acknowledgements

K. Wu acknowledged Dr Nicky Morden for her help in microtome, Dr Mehmet Davrandi for his help in antimicrobial result analysis.

References

1 A. Kramer, I. Schwebke and G. Kampf, *BMC Infect. Dis.*, 2006, **6**, 130.
2 World Health Organization, The Burden of Health Care Associated Infection Worldwide, 2010.
3 D. J. Anderson, D. G. Pyatt, D. J. Weber, W. A. Rutala and N. Carolina, *Am. J. Infect. Control*, 2013, **41**, 764–768.
4 R. D. Scott II, The Direct MeDical Costs of Healthcare-Associated Infections in U.S. Hospitals and the Benefits of Prevention, 2009.
5 OECD/EU, Health at a Glance: Europe 2016 – State of Health in the EU Cycle, Paris, 2016.
6 S. Noimark, J. Weiner, N. Noor, E. Allan, C. K. Williams, M. S. P. Shaffer and I. P. Parkin, *Adv. Funct. Mater.*, 2015, **25**, 1367–1373.
7 S. K. Sehmi, S. Noimark, J. C. Bear, W. J. Peveler, M. Bovis, E. Allan, A. J. MacRobert and I. P. Parkin, *J. Mater. Chem. B*, 2015, **3**, 6490–6500.
8 E. Ozkan, C. C. Crick, A. Taylor, E. Allan and I. P. Parkin, *Chem. Sci.*, 2016, **7**, 5126–5131.
9 W. J. Peveler, S. Noimark, H. Al-Azawi, G. B. Hwang, C. R. Crick, E. Allan, J. B. Edel, A. P. Ivanov, A. J. MacRobert and I. P. Parkin, *ACS Appl. Mater. Interfaces*, 2018, **10**, 98–104.
10 Q. Xu, X. Li, Y. Jin, L. Sun, X. Ding, L. Liang, L. Wang, K. Nan, J. Ji, H. Chen and B. Wang, *Nanoscale*, 2017, **9**, 19245–19254.
11 V. J. Suhardi, D. A. Bichara, S. J. J. Kwok, A. A. Freiberg, H. Rubash, H. Malchau, S. H. Yun, O. K. Muratoglu and E. Oral, *Nat. Biomed. Eng.*, 2017, **1**(6), 80.
12 S. K. Sehmi, S. Noimark, J. Weiner, E. Allan, A. J. Macrobert and I. P. Parkin, *ACS Appl. Mater. Interfaces*, 2015, 22807–22813.
13 M. Musterman, P. Placeholder, A. Santana Cruz, J. Flores, R. Guerra, C. Felipe and E. Lima, *Open Chem.*, 2018, **16**, 122–135.
14 S. Noimark, J. Weiner, N. Noor, E. Allan, C. K. Williams, M. S. P. Shaffer and I. P. Parkin, *Adv. Funct. Mater.*, 2015, **25**(9), 1367–1373.
15 S. Noimark, E. Allan and I. P. Parkin, *Chem. Sci.*, 2014, **5**, 2216.
16 T. J. Macdonald, K. Wu, S. K. Sehmi, S. Noimark, W. J. Peveler, H. du Toit, N. H. Voelcker, E. Allan, A. J. MacRobert, A. Gavriilidis and I. P. Parkin, *Sci. Rep.*, 2016, **6**, 39272.
17 S. Noimark, M. Bovis, A. MacRobert, A. Correia, E. Allan, M. Wilson and I. Parkin, *RSC Adv.*, 2013, **3**, 18383.
18 C. S. Oliveira, R. Turchiello, A. J. Kowaltowski, G. L. Indig and M. S. Baptista, *Free Radicals Biol. Med.*, 2011, **51**, 824–833.
19 S. Noimark, E. Salvadori, R. Gómez-Bombarelli, A. J. MacRobert, I. P. Parkin and C. W. M. Kay, *Phys. Chem. Chem. Phys.*, 2016, **18**, 28101–28109.
20 S. Noimark, C. W. Dunnill and I. P. Parkin, *Adv. Drug Delivery Rev.*, 2013, **65**, 570–580.
21 S. Noimark, C. W. Dunnill, C. W. M. Kay, S. Perni, P. Prokopovich, S. Ismail, M. Wilson and I. P. Parkin, *J. Mater. Chem.*, 2012, **22**, 15388.
22 S. Perni, P. Prokopovich, C. Piccirillo, J. Pratten, P. Parkin and M. Wilson, *J. Mater. Chem.*, 2009, **19**, 2715–2723.
23 K. Zheng, M. I. Setyawati, D. T. Leong and J. Xie, *ACS Nano*, 2017, **11**, 6910.
24 G. B. Hwang, H. Huang, G. Wu, J. Shin, A. Kafizas, K. Karu, H. Du Toit, A. M. Alotaibi, L. Mohammad-Hadi, E. Allan, A. J. MacRobert, A. Gavriilidis and I. P. Parkin, *Nat. Commun.*, 2020, **11**, 1–10.
25 S. Sharma, J. Bijwe, S. Panier and M. Sharma, *Wear*, 2015, **332–333**, 863–871.
26 A. L. Forster, A. M. Forster, J. W. Chin, J.-S. Peng, C.-C. Lin, S. Petit, K.-L. Kang, N. Paulter, M. A. Riley, K. D. Rice and M. Al-Sheikhly, *Polym. Degrad. Stab.*, 2015, **114**, 45–51.
27 E. M. Brach, D. Prever, A. Bistolfi, A. Pierangiola, B. Ae and L. Costa, *J. Orthop. Traumatol.*, 2009, **10**, 1–8.
28 J. Charnley, *Lancet*, 1963, **282**, 1379.
29 K. Wu, S. P. Douglas, G. Wu, A. J. Macrobert, E. Allan, C. E. Knapp and I. P. Parkin, *J. Mater. Chem. B*, 2019, **3310**, 3310.

30 D. D. Side, V. Nassisi, E. Giuffreda, L. Velardi, P. Alifano, A. Talà and S. M. Tredici, *Nucl. Instrum. Methods Phys. Res., Sect. B*, 2014, **331**, 172–175.
31 J. S. Chen, Z. Sun, P. S. Guo, Z. B. Zhang, D. Z. Zhu and H. J. Xu, *J. Appl. Phys.*, 2003, **93**, 5103–5108.
32 R. K. Sharma, M. Agarwal and K. Balani, *Mater. Sci. Eng., C*, 2016, **62**, 843–851.
33 A. M. Maley and J. L. Arbiser, *Exp. Dermatol.*, 2013, **22**, 775–780.
34 R. S. Traboulsi, P. K. Mukherjee, J. Chandra, R. A. Salata, R. Jurevic and M. A. Ghannoum, *Antimicrob. Agents Chemother.*, 2011, **55**, 3043–3045.
35 K. J. Farid, K. Kelly and S. Roshin, *Geriatr. Nurs.*, 2011, **32**, 85–95.
36 N. Lewinski, V. Colvin and R. Drezek, *Small*, 2008, **4**, 26–49.
37 C. Y. Tay, Y. Yu, M. I. Setyawati, J. Xie and D. T. Leong, *Nano Res.*, 2014, **7**, 805–815.
38 S. M. Kurtz, in *UHMWPE Biomaterials Handbook*, ed. S. M. Kurtz, Elsevier, 3rd edn, 2009, pp. 7–20.
39 S. Perni, C. Piccirillo, J. Pratten, P. Prokopovich, W. Chrzanowski, I. P. Parkin and M. Wilson, *Biomaterials*, 2009, **30**, 89–93.
40 H. Huang, G. B. Hwang, G. Wu, K. Karu, H. Du Toit, H. Wu, J. Callison, I. P. Parkin and A. Gavriilidis, *Chem. Eng. J.*, 2020, **383**, 123176.
41 S. Herbert, A.-K. Ziebandt, K. Ohlsen, T. Schäfer, M. Hecker, D. Albrecht, R. Novick and F. Götz, *Infect. Immun.*, 2010, **78**, 2877–2889.
42 S. Perni, J. Pratten, M. Wilson, C. Piccirillo, I. P. Parkin and P. Prokopovich, *J. Biomater. Appl.*, 2011, **25**, 387–400.
43 T. Kim, S. Jeon, D. Kwak and Y. Chae, *Fibers Polym.*, 2012, **13**, 212–216.
44 S. M. Kurtz, *UHMWPE Biomaterials Handbook*, 3rd edn, 2009, pp. 1–6.
45 M. C. Sobieraj and C. M. Rimnac, *J. Mech. Behav. Biomed. Mater.*, 2009, **2**, 433–443.
46 V. B. Gupta and V. K. Kothari, *Manufactured Fibre Technology*, ed. V. B. Gupta and V. K. Kothari, Springer, Netherlands, 1st edn, 1997, ch. 10, p. 225.
47 S. Rastogi, L. Kurelec and P. J. Lemstra, *Macromolecules*, 1998, **31**, 5022–5031.
48 K. Balani, V. Verma, A. Agarwal and R. Narayan, *Biosurfaces: A Materials Science and Engineering Perspective*, 1st edn, 2014, pp. 329–344.
49 DSC|hydrates, http://www.hydrateweb.org/dsc, accessed 19 June 2019.
50 E. Ozkan, F. T. Ozkan, E. Allan and I. P. Parkin, *RSC Adv.*, 2015, **5**, 8806–8813.
51 BSI Standards Publication, Light and lighting—Lighting of work places Part 1: Indoor work places, 2011.

